Michigan Technological University

Digital Commons @ Michigan Tech

Dissertations, Master's Theses and Master's Reports

2016

DESIGN AND DEVELOPMENT OF OPTICAL ELASTOGRAPHY SETUP

Abhinav Madhavachandran
Michigan Technological University, amadhava@mtu.edu

DESIGN AND DEVELOPMENT OF OPTICAL ELASTOGRAPHY SETUP

By

Abhinav Madhavachandran

A THESIS

Submitted in partial fulfillment of the requirements for the degree of

MASTER OF SCIENCE

In Biomedical Engineering

MICHIGAN TECHNOLOGICAL UNIVERSITY

2016

This thesis has been approved in partial fulfillment of the requirements for the Degree of MASTER OF SCIENCE in Biomedical Engineering.

Department of Biomedical Engineering

Thesis advisor: *Dr. Sean J. Kirkpatrick*

Committee member: *Dr. Keat Ghee Ong*

Committee member: *Dr. Jingfeng Jiang*

Department Chair: *Dr. Sean J. Kirkpatrick*

TABLE OF CONTENTS

LIST OF FIGURES

ACKNOWLEDGEMENT

I would like to thank Dr. Sean J. Kirkpatrick for guiding and supporting me through my career path and steering me in the right direction.

I thank Mitch Kirby for teaching me the basics of optics and imaging. I thank Basil James for lending a helping hand throughout the development of this project. Also, I would like to thank my friends, Dr. Andrew DeRouin, Salil Sidharthan, Govindan Suresh and Praharsh MV, at Biosensors laboratory for helping with the development of the project.

I would like to thank Dr. Keat Ghee Ong and Dr. Jingfeng Jiang for accepting to be my committee members.

I would like to thank my family, especially my parents, Madhava Chandran S and Krishna for providing me with unconditional love and support. I would like to thank Pooja, my sister Anna, my friends at Kri Nga Do and John for their support and encouragement in completing this thesis.

Above all, I would like to thank God for this wonderful opportunity to develop science and give back to the society.

ABSTRACT

The mechanical properties of the skin are an indication of its physiological condition. The properties can serve as potential information for dermatologists for diagnosis and qualitative assessment. Elastography is a medical imaging modality developed to extract the elastic properties of a tissue by application of an external force. Optical elastography is a technique of elastography which uses laser speckle tracking to study the elastic properties of several soft tissue including skin.

This work is aimed at developing an optical elastography setup that can study the elastic properties of skin. The setup includes an imaging system and a force-application system controlled by a user-friendly Graphical User Interface(GUI). This thesis describes, in detail, the hardware and software components involved in the setup and also, the results obtained with the use of this setup.

CHAPTER 1

INTRODUCTION

1.1 ELASTOGRAPHY

Elastography is a technique of medical imaging which maps the elastic properties of soft tissue. The stiffness of the tissue gives diagnostic information about itself. It acts as a sign of a pathological condition affecting the tissue [1]. A stiffer tissue is an indication of a tumor, malignant or non – malignant. For example, the detection and characterization of breast cancer is more elementary with the use of an elastography technique. Palpation is the most common and primitive method for understanding the changes in the stiffness of the tissue. But the ability to detect small tumors using palpation is limited. Hence, several non-invasive methods for elastography are available to provide stiffness information in a more systematic and quantitative manner.

The basic method of elastography involves applying a mechanical force to the tissue, internally or externally, and imaging the stiffness by analyzing the spatial deformation caused by the stimulation over a period of time. Strain, stress and the Young's Modulus can be estimated from the obtained data. There are various techniques that are utilized for elastography. Choosing the required technique depends on factors like penetration depth and resolution. The most prominent techniques of elastography include ultrasonic elastography, magnetic resonance elastography and optical elastography.

1.1.1 Ultrasonic elastography

Based on high frequency compressional waves or ultrasound waves, morphological images of organs can be re-constructed. The technique computes the difference between pre-compressed and post-compressed ultrasound signals to calculate the axial displacement occurring in the tissue [4]. The ultrasonic elastography is classified into quasi-static method and dynamic method on the basis of application of the external force.

Quasi-static method involves application of constant stress on the required region. The two-dimensional cross-correlation of the ultrasound images yield the displacement and the strain generated by the applied load [4]. The drawback associated with this method is that it is difficult to find the Young's Modulus since the stress distribution is unknown. This technique is hence considered qualitative [5].

Dynamic method involves application of time varying force which can either be a short transient mechanical force or an oscillatory force of fixed frequency. The shear waves which are basically low frequency (10Hz to 2000Hz) mechanical waves are directly proportional to the shear modulus of the medium [5]. The dynamic method can yield quantitative and higher resolution Young's Modulus mapping when compared to the quasi- static method.

Ultrasound elastography is also classified into Quasi- static method elastography, Vibro-acoustography and transient elastography method on the basis of the technique used.

Quasi-static elastography: This technique is an application of the quasi-static method in which static compression is applied on tissue and strain mapping is calculated from the difference between the

reference image and the image taken after compression. The 2-D correlation of the ultrasound images yields the displacement and strain. This technique is used in breast lesion characterization [6]. The absence of quantification is a drawback when the technique is considered.

Vibro-acoustography: This technique of ultrasound elastography is based on radiation pressure, which is a volume force developed by the transfer of momentum, that is proportional to the absorption of ultrasound waves in the medium [7]. It uses the transmission of two confocal ultrasound waves to create a modulated force which produce beats which are used to deduce the mechanical stiffness of the medium. An entire area is swept in order to get a mapping of the stiffness. The drawback regarding this technology is that the sweeping, to create a stiffness mapping, takes a long acquisition time making this technique difficult to be implemented in real-time.

Acoustic Radiation Force Impulse Imaging (ARFI): This technique of ultrasound elastography makes use of acoustic radiation force with one confocal ultrasound beam. Making use of ultrasound-speckle tracking, the imaging system tracks the speckle focal point thus deducing displacement. The speckle tracking in ultrasound technology can track the displacement by correlation of each consecutive windows of ultrasound data to determine of displacements even less than a micrometer [8]. The ARFI Imaging technique can produce displacement mapping of the medium by sweeping the zone. This can cause heating due to deposited energy in the medium and longer acquisition time making it difficult for real-time imaging.

Shear wave/ Transient elastography: This technique is based on measuring the velocity of the shear waves that are propagated into the soft tissue. There are two kinds of transient elastography which are 1D transient elastography and 2D transient elastography. The displacement generated from the force of the shear wave is estimated using correlation of retro-diffused waves [9]. It is recorded at a high frame rate at about 5000 frames/second to around 20,000 frames/second with a mono-dimensional ultrasound transducer [10].

1.1.2 Magnetic resonance elastography

This method utilizes a special Magnetic Resonance Imaging (MRI) technique to assess the propagation of mechanical waves through a medium thus deducing the stiffness of the medium. Magnetic Resonance Elastography (MRE) uses mechanical shear waves of a single frequency which are synchronized with the magnetic resonance pulse sequence. A magnetic resonance imaging technique called phase contrast MRI is used to image the tissue motion due to the propagation of the shear waves. This technique is based on conventional MRI [11].

MRE is capable of imaging deeper into the tissue which helps in recreating the 3D structure of the tissue and the contrast resolution. Since low frequency shear waves are used to increase the penetration depth, resolution is affected. This adversely affects the capability of detecting pathological conditions at a small scale. Also, MRE is expensive when compared to other modalities used for elastography.

1.1.3 Optical elastography

This technique makes use of coherent-light based methods in order to obtain the mechanical stiffness of the skin. Laser speckle

technique used for the mechanical characterization of tissue has many advantages of being non-contact, non-invasive as well as in providing high resolution [12]. This method is aimed at computing relative strain in tissue by tracking the laser speckle pattern obtained by illumination of coherent light on the deformed tissue.

Optical elastography has an advantage of being non-invasive and provides higher spatial resolution when compared to other modalities used for elastography. This can also offer increased strain resolution on the order of a single micro-strain [13]. However, optical elastography has a disadvantage of lesser penetration depth compared to other modalities. The penetration depth of optical elastography methods are limited to a few millimeters beneath the skin. In order to overcome this limitation, several techniques like endoscopy and needle-based probes are used in conjunction with the usual methods of optical elastography.

Optical elastography is done by tracking the speckle pattern obtained by illuminating the region of interest during the application of deformation. A reference image of the speckle pattern before deformation is acquired and then the movement in the speckle pattern due to deformation is tracked by acquiring subsequent images for each stage of deformation. The tracking of the speckle pattern is done by image processing algorithm which gives the corresponding relative strain that occurred in the region of interest due to deformation. High speed sampling of the speckle pattern is required to track the movement during deformation and hence, the system requires to acquire speckle images at a high frame rate.

There are many different applications for optical elastography among which dermatology, oncology and ophthalmology are the leading areas of application.

Dermatology: Application of light-based method is suitable for the skin since the penetration depth of the light is limited and the resolution is high. Changes in the mechanical stiffness of the skin can be due to several diseases or pathological conditions associated with the skin. Skin tumors which are present in the subsurface can alter the mechanical stiffness compared to the normal tissue surrounding it. Acousto-optical elastography technique have demonstrated mechanical stiffness in micro-scale for both mouse melanoma lesion and human melanocytic nevi [14].

Oncology: The application of optical elastography in oncology is very promising due to its high resolution. The limited penetration depth and high resolution makes optical methods better for some aspects of cancer treatment. During surgical removal of cancer tissue, optical elastography can be used to ensure complete removal as it is a fast and better modality in identifying remaining malignant tissue. Due to its high resolution, it can distinguish between microstructures of malignant tissue and healthy tissue [15].

Ophthalmology: Mechanical stiffness in the eye is an identifier of the several diseases such as glaucoma, keratoconus and presbyopia. There are several optical elastography techniques that apply force on the cornea in order to study the mechanical stiffness of the cornea. Several methods like air puff mechanism or photo-thermal expansion by pulsed laser are used to induce mechanical displacement in the cornea. The non-contact optical elastography method is a better diagnostic tool for ophthalmology.

Cardiology: The characterization of atherosclerotic plaques is an important part in the identification of a pathological condition related to cardiology. Optical elastography method provides a greater resolution when compared to modalities like ultrasound elastography. Optical elastography probes are designed and developed in order to image the internal walls of the vascular structure which can help in the identification and characterization of atherosclerotic plaques [16].

1.2 SKIN BIOMECHANICS

Human skin is composed of epidermal and dermal layers, each with its own functional importance. The mechanical properties of skin depend on the properties of these different layers that form the skin. Aging and diseases affect the skin by changing the mechanical properties of different layers. Collagen and elastin are the main components of the skin and the major changes in the mechanical properties of the skin are due to these components.

Collagen is an important structural component in the skin which provides tensile strength to the skin. Collagen weighs around 70 to 80% of the total dry weight. There are several diseases like scleroderma and scleredema which affects the metabolism of collagen. It causes the thickening of collagen leading to increased stiffness in the skin [24]. Diabetic thick skin is another disease that affects the metabolism of collagen by increasing the thickness of the skin. Conversely, in skin-atrophy, reduced synthesis of collagen takes place leading to the thinning of skin.

The elastic fibers in the dermis are arranged as a three dimensional network. The elastic fibers are composed of an amorphous material called elastin. Cutis-laxa is a skin disease that damages the elastic fiber and presents as predominant wrinkling [25].

Diseases like Anetoderma and Elastoderma causes degradation and accumulation of elastic fibers respectively, thus affecting the elasticity of the skin.

Aging is another factor that affects the elasticity of the skin. As age increases, the dermal elastic fibers become thicker and fragmented. [26] Disintegration of elastic fibers in the aged skin leads to slower elastic recovery in elderly people [27].

The change in the elasticity or stiffness of the skin is a sign or symptom of the ongoing pathological condition in the skin. Optical elastography is a promising technique to study the changes in the mechanical behavior of the skin.

1.3 MECHANICAL STIFFNESS OF SKIN

Skin is composed of mainly three layers: Epidermis, Dermis and Hypodermis. The Young's Modulus is an important parameter that can state the characteristics of the skin. The mechanical testing of the skin is used to understand the mechanical properties particularly stiffness of the skin, the results of which can be used to understand the pathological conditions of the skin. Several diseases like Scleroderma, Morphea and Radio dermatitis change the mechanical properties of the skin affecting its stiffness. Hardness, elasticity and viscosity of the skin can be factor to understand conditions like systematic sclerosis [17].

There are different techniques for testing and understanding the mechanical properties of skin that employs different methods to change the shape of skin.

1.3.1 Tensile test

This is an ex-vivo or in-vivo test performed under controlled conditions. The skin is stretched in its own plane with a bi-axial or uni-axial load [18]. The observed non-linear relation between the strain and the applied stress yields the Young's modulus. Dynamic tensile testing is done to obtain Young's modulus at different stretch velocities in a range of 1-1.5 ms^{-1} [19]. An extensometer is an apparatus that is used to conduct tensile testing on the skin. The principle of an extensometer is that it applies known uniform extension on the skin. There are different types of extensometers like portable hand-held extensometer, magnetic extensometer and Cutech extensometer.

1.3.2 Indentation test

The indentation test is a method to study the biomechanical properties of the skin in-vivo. The method applies a perpendicular force on the region of interest with the use of an indenter. It treats skin as a monolayer and restricts the indentation amplitude to a few microns. The mechanical indentation in a perpendicular manner provides Young's Modulus in the perpendicular direction without any skin pre-stressing [20]. A tissue resonator indentation device (TRID) is used for dynamic analysis that resonates tissue at a frequency range of 0–500 Hz. In an advanced device called Tonoderm which is used to measure the Young's modulus on human forearm, the indentation is applied using an air compressor in which the depth and distance of indentation is measured using a laser displacement system [21]. A micro-indentometer is based on the principles of indentation where the indentation is done by a needle on the stratum corneum. The velocity of the indentation is proportional to viscosity as well as

stiffness of the medium. The deformation due to the indentation is dependent on these factors. The device uses a moving coil vibrator which incorporates a linear variable displacement transducer. It works by rapidly intending the stratum corneum to a maximum depth of 20 μm and reads the reaction force [22].

1.3.3 Suction test

Suction test makes use of suction pressure in order to study the mechanical properties of the skin. A Cutometer is a device which works on this principle. A pre-defined negative air pressure is created and applied on the skin by drawing air out of a diaphragm creating a vacuum pulling the skin to its aperture [22]. The vertical deformation of the skin due to the suction effect is measured using an optical system. The optical system includes a light transmitter, a receiver and two glass prisms that project infrared light from transmitter to receiver. The weakening of the intensity of the light is recorded by the receiver. This reduction in intensity is dependent on the penetration depth of light into the skin [22].

There are two measuring techniques for suction test, which are stress-strain mode and time-strain mode. In stress-strain mode, the vacuum is increased over a period of time and the deformation is recorded as a function of negative pressure. In time–strain mode, a defined vacuum is applied over a period of time and deformation is recorded as a function of time.

1.3.4 Torsion test

This test involves application of constant torque on the skin in order to obtain the mechanical stiffness of the skin. The torque is applied using a guard ring and an intermediary ring. The resultant rotation of

skin is measured. The method is used because it reduces the anisotropic effects as the underlying layers of skin does not take part in the rotation [23]. As the torque is applied, an immediate viscoelastic deformation occurs which is time dependent. In torsion, elongation is rotational which makes it more complex when compared to other modalities.

CHAPTER 2

THEORETICAL OVERVIEW

The two-dimensional optical elastography technique is based on analysis of static speckles. The movement in the speckles is estimated by matching the optical frames captured at high frame rate during the deformation.

2.1 LASER SPECKLE SHIFT ESTIMATOR

Laser speckle is an intensity pattern that is produced by mutual interference of a set of wavefronts [28]. It is basically produced by the interference of several waves of same frequency, but of different phase and amplitude. When a rough surface is illuminated using a coherent light, each point acts as a source for a secondary spherical wave. If the surface is rough enough to create a path-length difference, with phase changes greater than 2Π, the resultant light intensity varies randomly [29]. The resulting speckles when collected on an image plane with a lens and aperture mechanism are called subjective speckles. The speckles that are formed on the illuminated surface are called the objective speckles.

The coherent light waves, when penetrating inside a surface, undergo depolarization and decorrelation. Two different estimation schemes insensitive to these effects have been proposed for calculating speckle shifts [30].

Non-parametric speckle shifts: This algorithm estimates the shift in the speckle pattern by calculating the difference between the correlation peaks while analyzing sequential frames.

Parametric speckle shifts: This algorithm relies on priori assumption of the experiment. In case of a maximum likelihood shift estimator, two assumptions are made. One is that the speckle shift is smaller than the pixel size. Second is that the measured signal is a combination of deterministic speckle signal and noise. The signal obtained is represented by the equation,

$$s_j(x_i) = f_j(x_i) + n_j(x_i) \tag{1}$$

Where f_j is the speckle signal at j^{th} sequence.

x_i is the spatial dimension of pixel i.

n_j is the zero-mean noise term at j^{th} sequence.

By calculating the central difference about j^{th} data, the resulting equation takes form,

$$s_{j+1}(x_i + \delta x) - s_{j-1}(x_i - \delta x) = f_{j+1}(x_i + \delta x) - f_{j-1}(x_i - \delta x)$$
$$+ n_{j+1}(x_i + \delta x) - n_{j-1}(x_i - \delta x) \tag{2}$$

Where δx is the shift value in spatial domain.

By assuming a constant mean for the sequential speckle pattern and Gaussian distribution of zero mean and constant variance, the noise probability density function is given by [31]:

$$p(s_j | f_j) = p(n_j)$$
$$= C \exp\left\{ -\frac{1}{2\sigma^2} \sum_{i=1}^{N} \left[f_{j+1}(x_i + \delta x) - f_{j-1}(x_i - \delta x) \right]^2 \right\} \tag{3}$$

13

Where C is a constant. The δx that maximizes the likelihood function is as shown,

$$\frac{\partial}{\partial(\delta x)} \ln p\left(s_j \,|\, f_j\right) = 0$$

(4)

The equation gives an unbiased estimation of speckle shift pattern [30].

CHAPTER 3

MATERIALS AND METHODS

3.1 OVERVIEW

The elastography system comprises of optical, mechanical and electrical components. The main components of the system are as follows:

i)   532nm green laser with a power of 30mW.

ii)   Pointgrey CCD camera capable of capturing 200 frames/second.

iii)   An f/2.8 aperture C-mount lens with 55mm focal length.

iv)   20X Microscope objective

v)   CLIPPARD EVP air-valve

vi)   NI DAQ system

vii)   LabVIEW 'Optical Elastography' Graphical User Interface (GUI).

LASER setup

The Laser used in the setup is a 523 nm green laser with a maximum power of 30mW. The laser beam is diverged using a 20X Microscope objective in order to obtain a beam diameter greater 4 cm on the plane to be imaged. The microscope objective and a polarizer is aligned with the laser using an optical cage system. The entire laser system is screwed onto an adjustable optical breadboard. This enables a 3-axial adjustment of the laser system depending on the size and thickness of the subject's forearm.

Camera setup

The camera used in the setup is a Pointgrey Grasshopper CCD. The camera is capable of capturing images at the rate of 200 frames/second. The sensor used in the camera is a Kodak KAI0340 monochrome image sensor which has a maximum quantum efficiency at a range of 450 to 550 nm. The monochrome sensor increases the sensitivity of the camera.

A f/2.8 C-mount lens with a focal length of 55mm is used to focus the light from the image plane onto the image sensor. A polarizer is placed in front of the C-mount lens in between the object plane and the lens.

Pneumatic system

The air system which supplies controllable air pressure on the skin comprises of a CLIPPARD EVP air valve. The air valve is supplied variable voltage and current which opens the valve accordingly, thus controlling the air pressure. The valve is supplied a sinusoidal voltage signal of the range 0-5V using an NI DAQ system which is in turn controlled by a LabVIEW GUI. In order to drive the valve, the current from DAQ is amplified using a transistor and then supplied to the valve.

LabVIEW GUI

An important part of the project is the GUI that controls the air system and the camera acquisition at 200 fps. This GUI enables the user to set the amplitude and the frequency of the sinusoidal voltage signal being supplied to the valve. A live feed of the camera is displayed in the GUI which helps the user to adjust the image settings and the experimental setup/position before starting the acquisition.

The GUI enables the user to acquire the images in a frame based mode where the recording stops after a set number of frames are acquired and a normal recording mode where the user can start or stop recording.

The voltage being supplied to the valve is also shown in real time on the display above the camera live feed. In order to make sure that the recording starts for the same air pressure at each time, the sinusoidal voltage is reset at each time the record button is pressed.

MATLAB CODE

The MATLAB algorithm is used for the post-processing of the sequential images captured at 200 frames/second. The code outputs the relative displacement by tracking the speckle in each optical frame.

3.2 HARDWARE DESIGN

The hardware design of the system consists of five main blocks.

3.2.1 AIR SYSTEM

The air system is run by the LabVIEW GUI from where the voltage being supplied to the air valve can be controlled. A sinusoidal voltage with user-defined frequency and amplitude is supplied to an NI Digital Acquisition System (DAQ) which converts the digital signal into an analog sinusoidal signal. The signal is then fed into a current amplification system. The signal output from the current amplifier is then supplied to the valve to produce the sinusoidal air puffs. The metal tube carrying air is then placed at a distance of 1 cm from the skin in order to apply the force on the skin.

GUI controls

The LabVIEW GUI is designed to control the amplitude and the frequency being supplied to the air valve which in turn controls the air puff pressure and frequency.
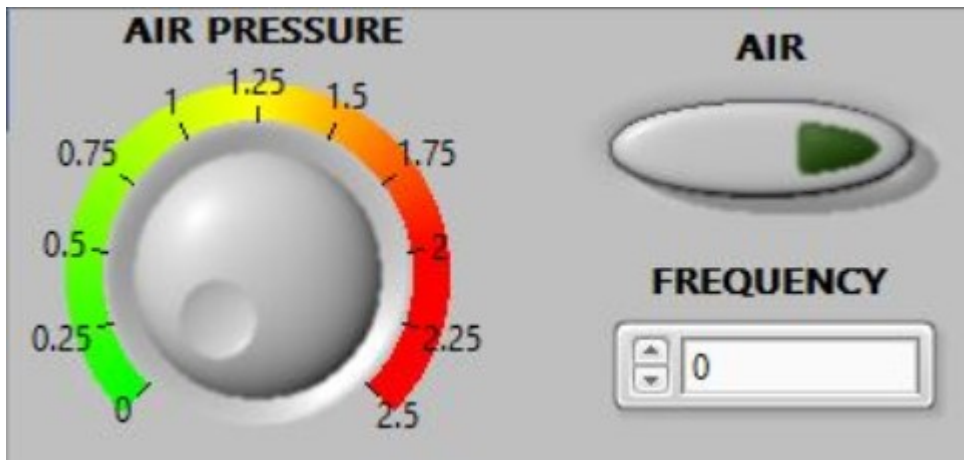

Figure 3.1: Air system GUI

The GUI has an amplitude knob which can be used to control the voltage being supplied to the air valve. A voltage from 0–2.5V with an offset of the same setting is supplied from the GUI to the DAQ in order to deliver a sinusoidal voltage of 0- 5V.

The frequency can be controlled by the numerical input dialog box which sets the frequency of the sinusoidal signal being supplied to the valve.

A display system is included in the GUI to visualize the signal being fed to the DAQ. The signal is generated at 100000 samples/second in order to equalize it with the sampling rate of the DAQ. Also the air signal resets itself each time a recording or acquisition starts.

EVP AIR VALVE

The air flow and pressure is controlled by the electronic valve which opens and closes according to the voltage supplied to it. The air valve used in this system is a CLIPPARD EVP proportional valve EC-P-05-25A0. It operates in a voltage range of 0–5 V DC with a current range of 0-370 mA. The valve is able to supply a pressure range of -5 to 100 psig.

The valve is connected to a 90 psig air supply and the other end is connected to a pipe which applies force on the region of interest at a fixed distance.

DAQ SIGNAL CURRENT AMPLIFICATION CIRCUIT DESIGN

The signal from the DAQ is used to drive the EVP air valve. Although the voltage of the sinusoidal signal ranges from the required voltage of 0-5V, the current supplied by the DAQ is around 5mA. This is not enough to drive the air valve. Hence a circuit was designed and setup in order to amplify the current in the signal produced from the DAQ. This amplified current is then supplied to the air valve.

The transistor used is a high-current NPN medium power transistor (ST 2SD882, ST electronics). The transistor is designed to work as a common-collector amplifier in order to amplify the current of the input signal. The input is fed into the base of the transistor and the valve is driven with the signal from across the emitter. The collector is supplied a voltage of 5V.
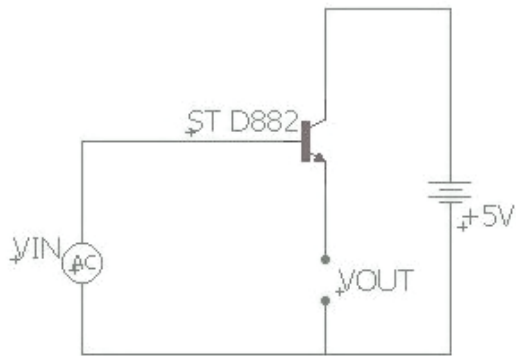
Figure 3.2: Common- collector amplifier configuration

The h$_{FE}$ or DC current gain of the transistor is specified by the manufacturer as 100 [35].

3.2.2 CCD SYSTEM

The CCD system is used to capture images of the area illuminated by laser at a high acquisition rate. The ideal acquisition rate for capturing every single movement of the speckle is 200 frames/second. The LabVIEW GUI is used to set the required attributes of the camera before start of the acquisition.

GUI controls

The GUI includes setting of camera attributes like saturation, brightness, gamma and exposure. The user can control and set the attributes to the required settings and press the SET button to set it before acquisition. The GUI also includes a real-time viewer which provides live feed of the camera in order to set the system in the required position. The SET button when pressed prompts the user to select a folder saving the images and video captured. The camera is set in the 200 fps mode in the NI MAX during initial installation. The

frame rate for the video can be selected which creates a video of the set frame rate with the frames captured at 200 frames/second.
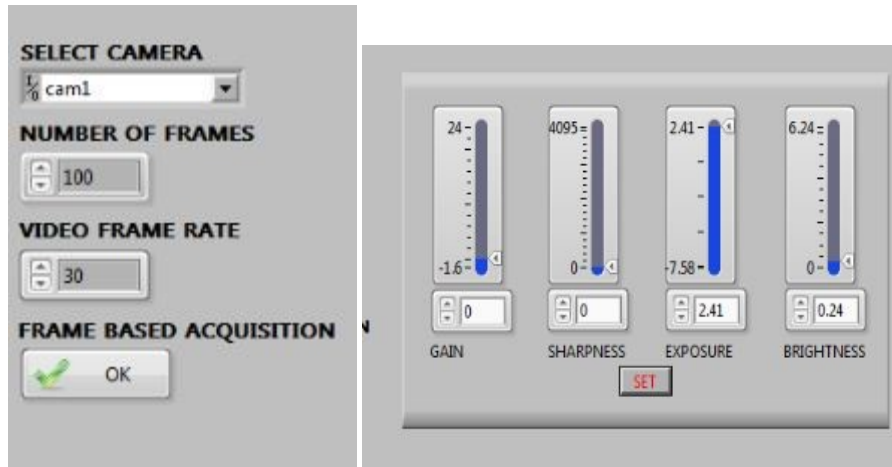

Figure 3.3: GUI controls for the CCD

Hardware

CCD Camera: The CCD camera is a Pointgrey Grasshopper 0.3 MP monochrome camera (GRAS-03K2M-C - Pointgrey). It is a Firewire-based camera with an IEEE 1394 connection for transmission of data between the camera and the computer. The camera has a CCD monochrome image sensor (Kodak KA10340) which is highly sensitive in the wavelength range of 450 -550 nm [32]. It is a global shutter CCD with the capability of capturing 200 frames/second depending on the processing power of the computer connected to it. The camera is capable of producing images with a resolution of 640 x 480. But it has a limited resolution of 320 x 240 when the camera is set to work in Mode 0 with a frame rate of 200 frames/ second.

C-mount lens:

The C-mount lens is used to direct the light from the object onto the image sensor. The C-mount lens is a crucial component of a speckle system as the subjective speckles are caused due to the aperture opening in the C-mount lens. It helps to focus the object plane and adjust the zoom of the image being captured. The C-mount lens used in this setup is a 55mm focal length lens with an aperture of f/1.8.

The C-mount lens is used is a tele-centric lens with an aperture stop of f/1.8 (Computar). The C-mount lens has a working distance of 140mm to infinity with a wide depth of field. It is suitable for use as a telephoto and as a macro lens.

According to Kirkpatrick *et.al,* speckle size should be at least twice the pixel size in order to satisfy the Nyquist's sampling criterion and maximize the contrast of the imaged speckle pattern [33]. In order to achieve this, the aperture is set between f/22 and f/32 where it is found out to satisfy the sampling criterion.

The magnification of the C-mount lens is adjusted in such a way that the region imaged is of dimension 2cm x 2.5cm. A polarizer is placed in the front of the C-mount lens in order to select linearly polarized light and to increase the contrast of the grabbed speckle [34]. The light that gets scattered off from the surface of interest has to be filtered out with a known angle of polarization which is set for the laser system.

Software

The camera is controlled by the LabVIEW GUI. As for an initial setting, the camera is accessed using NI-MAX (Measurement and Automation Explorer). This software can be used to interface the camera and select the mode in which the camera should work in. For the camera to acquire images at a frame rate of 200 frames/second, the Grasshopper camera should be set to Format 7, Mode 0 which sets the camera to a pre-defined setting for facilitating a 200 frame rate acquisition. This, however, drives down the resolution of the images from a 640 x 480 to 320 x 240 pixels. But, this does not affect the elastograms generated after post-processing.

The default camera attributes in Format 7, Mode 0 for acquiring at a frame rate of 200 are as follows:

Gain: 0

Sharpness: 0

Exposure: 2.41

Brightness: 0.24

The camera is then accessed by LabVIEW GUI using the built-in IMAQdx library which lets the GUI control the camera and record the images.

3.2.3 LASER SYSTEM

The laser system is a stand-alone system which is not controlled by the GUI consisting of a 532nm green laser, a microscope objective and a linear polarizer. The laser used for the purpose is a green 532 nm laser with a maximum power of 30 mW under the regulations of clinical laser use by the FDA. The laser with 532 nm is chosen so as to limit the penetration depth to the upper layers of the skin and to avoid the data in the depth of the skin. Since the setup is to study the application of cosmetics, the effects on stratum corneum and epidermis are studied. The laser beam is diverged using a microscope objective of 20X magnification. This expands the laser beam in order to uniformly illuminate the region of skin to be imaged. A polarizer is placed between the skin and the beam in order to transmit the linearly polarized light in a known angle of polarization.

3.2.4 ARM RESTRAINING SYSTEM

In order to set the skin in the focal plane of the camera, the hand is placed on a height-adjustable mount. The hand is supported by a bean bag which provides comfort to the subject and also restrains the hand from excessive movement that could affect the data collected.

3.2.5 LOAD CELL AIR PRESSURE MEASUREMENT SYSTEM

A load cell (FN 3148, Measurement Specialties) which has a full scale range of 50N is used to measure the force exerted by the air system on the region of interest to be imaged. Based on Wheatstone's bridge principle, the load cell is supplied an excitation voltage of +/- 10 V and has a full scale output of +/- 2mv/V. The load cell has a zero offset less than +/- 5% of full scale. The load cell is driven by a Weight

sensor system (MM45 Load-cell Readout, Entran) which supplies the required excitation voltage and amplifies the output voltage.

The load cell is tested for accuracy and reproducibility by testing it three times with known weights. The voltage from the load cell read out is measured using an oscilloscope with known weights. Also, the voltage generated by the load cell with the application of air pressure is measured using the oscilloscope for different DC voltage supplied to the valve.

3.3 SOFTWARE DESIGN

The software for the setup includes a LabVIEW GUI and a MATLAB code. The LabVIEW GUI acts as a user interface in order to control the different systems and record the raw images. The MATLAB code is used to process the raw images to obtain the elastograms and the displacement data.

3.3.1 LABVIEW GUI

The LabVIEW GUI is designed to control the CCD system and the air system in a user friendly manner. The camera settings are pre-defined by the NI MAX software in order to achieve a frame rate of 200 frames/second. The flowchart for the GUI code is as shown in figure 3.4.
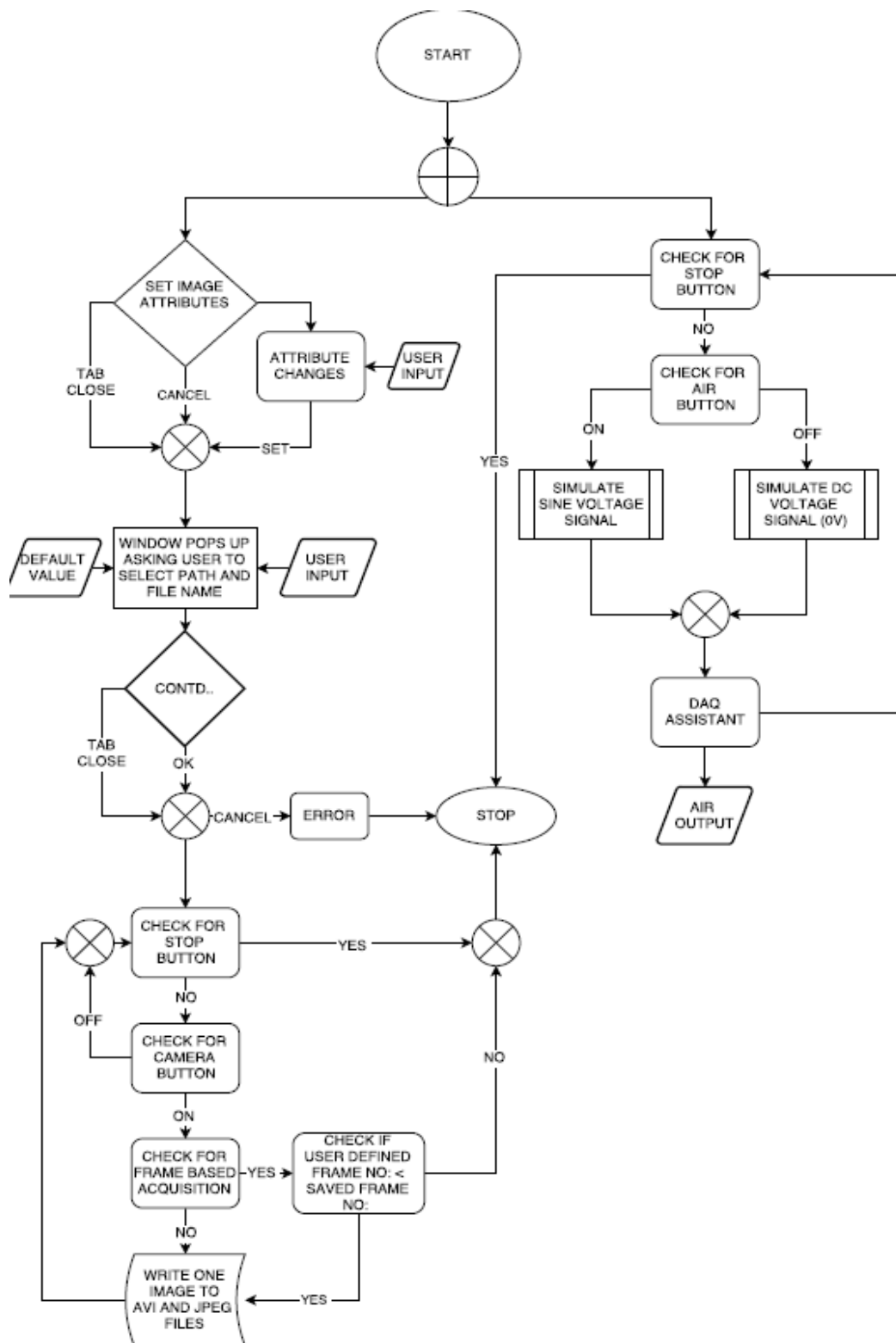
Figure 3.4: Flowchart for LabVIEW GUI.

There are two different blocks in order to control the CCD system and the Air system separately.

CCD system block

A flat structure sequence is used in the CCD system GUI programming. The flat structure sequence enables the sub-diagrams or frames to execute sequentially. The data from one frame leaves each frame when the execution is complete.

The first sequence is programmed for camera initialization. The first sequence is as shown in Figure 3.5. A session in block is used to specify the camera to be used. A user prompt dialog box is programmed to let the user set the camera attributes such as exposure, gain, sharpness and brightness.
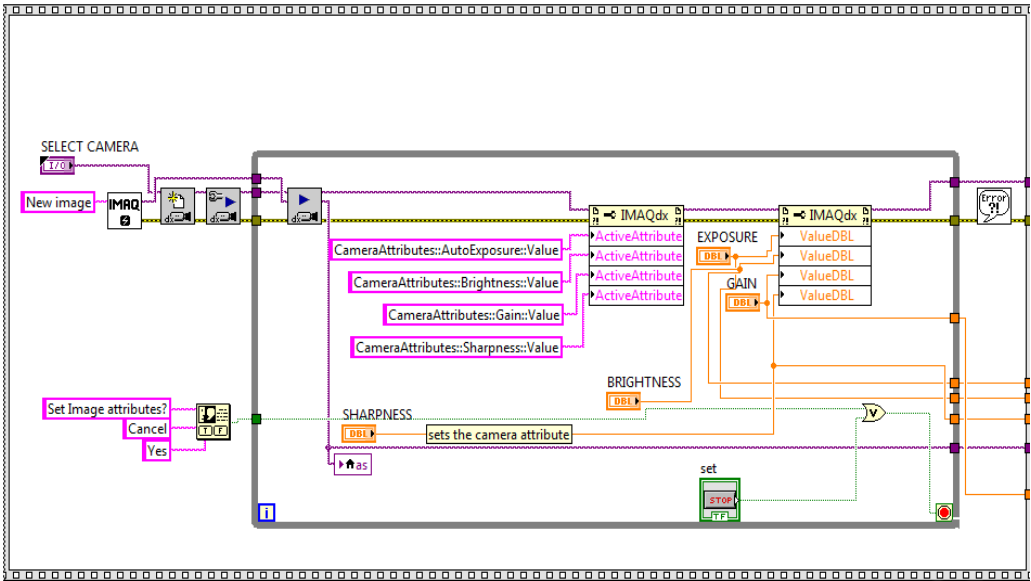
Figure 3.5. First sequence block diagram

The second sequence, which is the acquisition sequence is as shown in Figure 3.6. The second sequence is programmed to prompt the user to select or create a folder to save the images and video that

are to be acquired. Also, it has a file create and write module that creates a file in the saved folder with the timestamp details and comments by the user. The second sequence also hosts the while loop for the acquiring the images and saving them in the folder specified by the user.
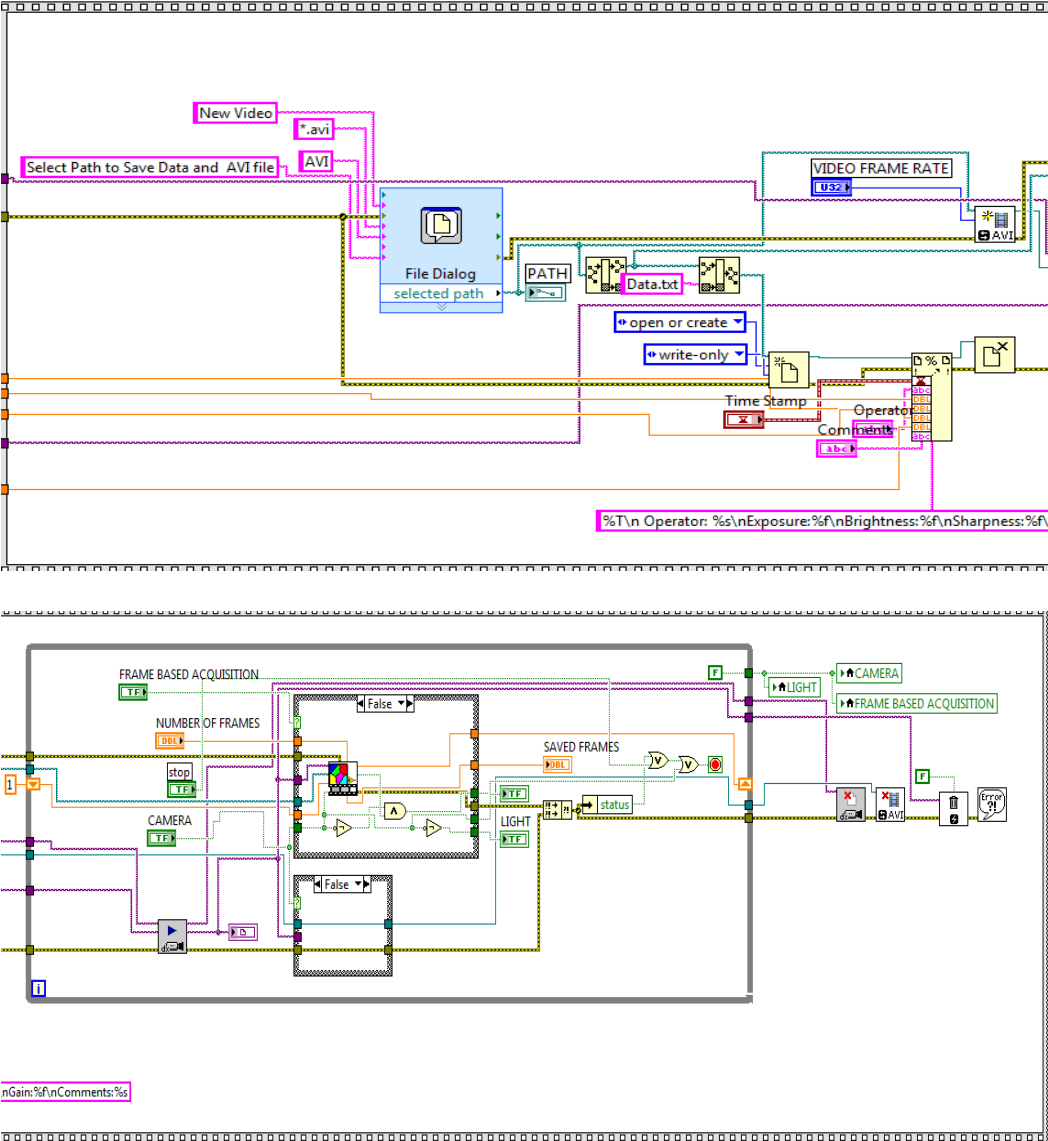

Figure 3.6: a) File creation block in the second sequence b) Image acquisition block in the second sequence.

The images captured are saved and named using a sub VI as shown in Figure 3.7 which is programmed inside the acquisition while loop. For frame-based capture mode, the acquisition sequence is halted if the number of frames set by the user has been achieved. Also it is programmed to stop if the user changes commands by clicking the record button.
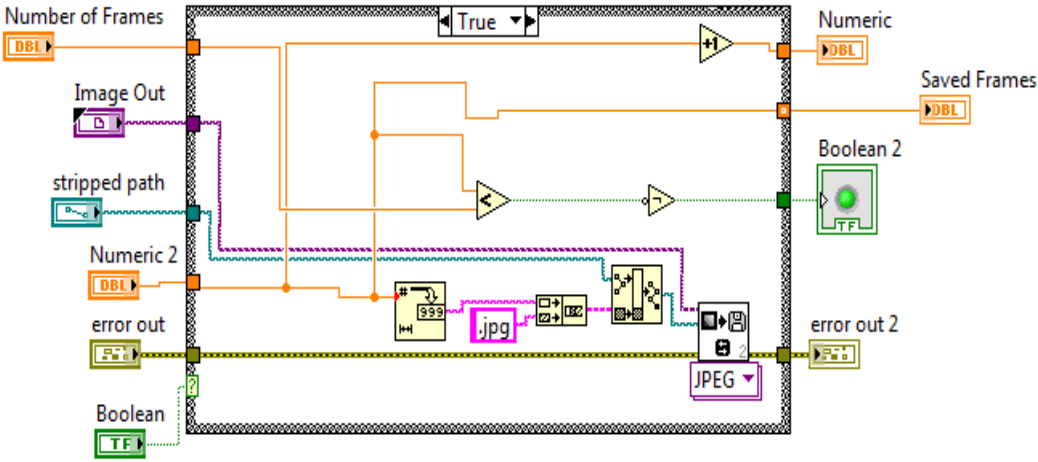

Figure 3.7: File saving VI block diagram

Air system

A while loop structure is used in the Air system GUI programming. The block diagram for the Air system block is as shown in Figure 3.8. The air system includes a Simulate signal block which is linked to the input of a DAQ Assistant which outputs the signal through the Analog output (A0) pin of the DAQ. The simulate signal VI is set to produce sinusoidal signals with a user-defined frequency and amplitude. This enables the user to control the amplitude and the frequency of the sinusoidal wave being fed to the air valve.
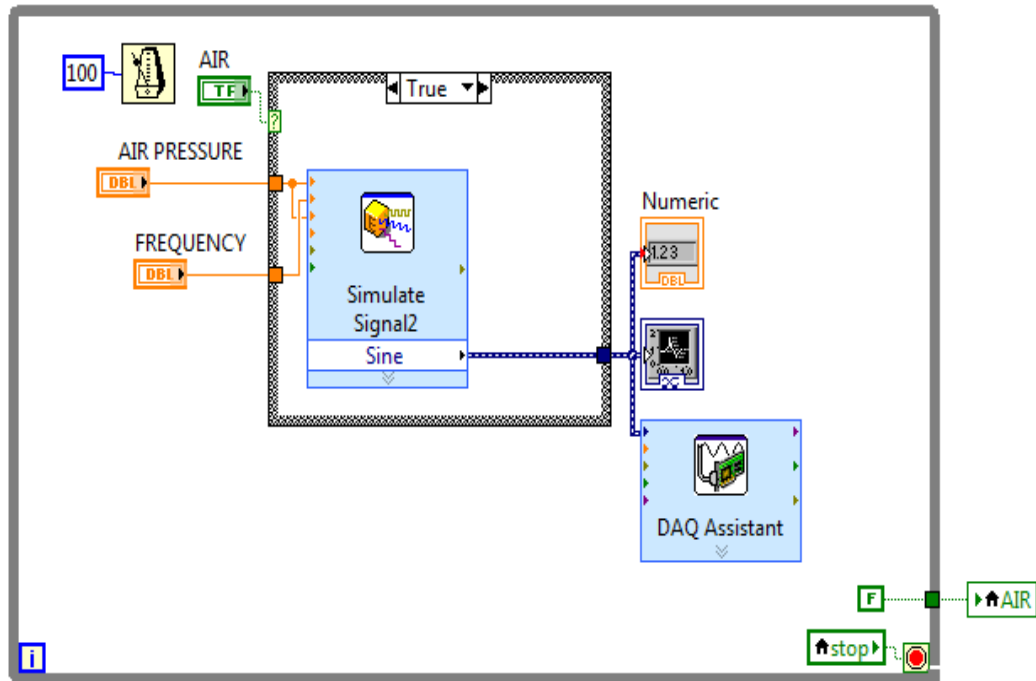
Figure 3.8: Air system block diagram

3.4 METHOD

3.4.1 MEASUREMENT OF APPLIED FORCE

LOAD CELL TESTING (WEIGHT VS VOLTAGE)

- The load cell is setup by connecting it to the load cell read out.
- The known weights ranging from 2 grams to 20 grams are placed on top of the load cell.
- The output from the load cell is read using an oscilloscope for each weight.
- The weights are converted to force in kilogram-force for corresponding voltage.

FORCE VS VOLTAGE DATA

- The load cell is positioned at 1 cm below the air-pipe in order to apply force at an angle of 30° on the top of the load cell.

- Different set of DC voltage is set in the LabVIEW GUI to drive the valve.
- The voltage from the load cell read out is measured using an oscilloscope.
- The force corresponding to the read out voltage is plotted with the voltage supplied to the valve.
- The range of force supplied by the air system is thus calculated.

3.4.2 PREPARATION

- The inner upper arm of the subject/ volunteer is positioned on the height- adjustable base.
- The arm is positioned so that the subject is in a relaxed state and the area of skin to be imaged is in the focal plane of the camera. A bean bag is placed under the arm in order to prevent unnecessary movement in the arm.
- Three sets of base images, without application of any substance, is taken with each set containing 200 images.
- After the acquisition of base images, outline of the area to be imaged is marked on the skin of the volunteer. The outline is a rectangular region of 3 cm x 2.5 cm with a diagonal to divide the area in to two equal triangles. The area imaged is a region of size 2 cm x 1.5 cm within the marked region.
- Half of the area marked is smeared with the substance to be tested. The other half is left without application of any substance.
- The arm is positioned again in the focal plane in such a way that the air pipe is pointed towards the corner of the square marked on the skin. This ensures that the force applied on the

skin by the air is equal on both the treated and non–treated sides.

3.4.3 ACQUISITION AND IMAGE PROCESSING

- The GUI is launched in order to set the arm position with the air pipe positioned at the corner of the imaging area for equal distribution of force to the treated and non-treated area.

- The air pressure is set at required force and frequency and then turned on.

- The camera attributes are set in order to get required brightness, gain, sharpness and exposure. The user can select the folder for storage of the images captured when prompted.

- The required recording mode (Frame based acquisition/Normal recording) is selected.

- The images are captured at 200 frames/second.

- The images for each acquisition is loaded in to a MATLAB code. The MATLAB code outputs the displacement caused in the area being imaged.

- The code outputs cumulative displacement in the x direction and y direction and cumulative vector displacement.

CHAPTER 4

RESULTS

4.1 CURRENT AMPLIFIER

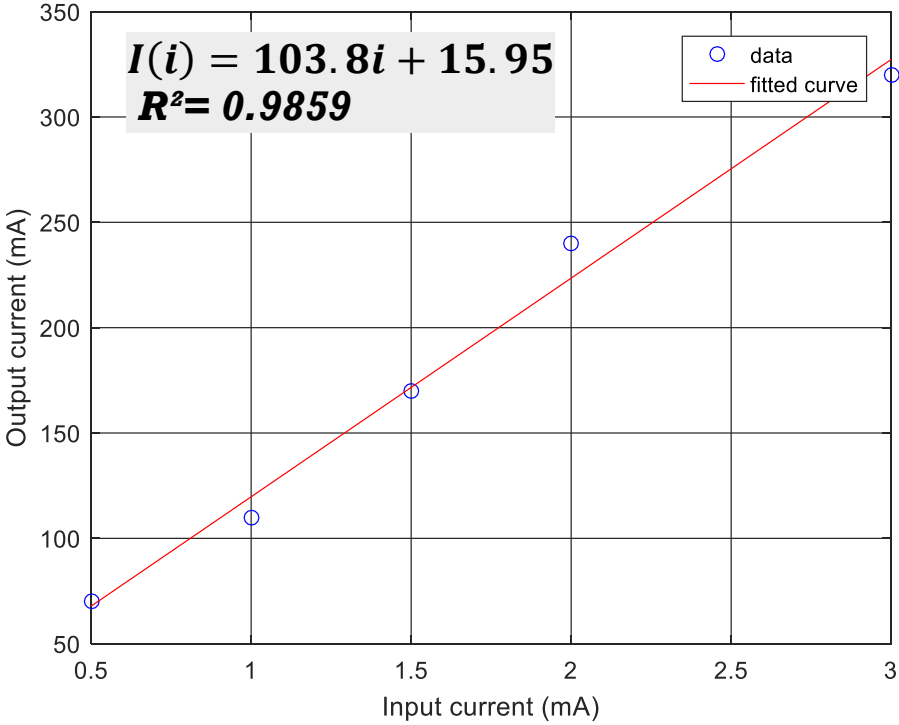$I(i) = 103.8i + 15.95$
$R^2 = 0.9859$

Fig 4.1: Current amplifier amplification curve

The experimentally derived current gain of the current amplifier is as shown in Figure 4.1. The current gain is closer but slightly above 100. The response of the transistor amplification is a linear fit of an R-squared of 0.9859. The change in the experimentally obtained gain from the calculated gain from the specification might be due to the temperature changes and the difference in the collector-emitter voltage of the transistor.

4.2 LOAD CELL TEST
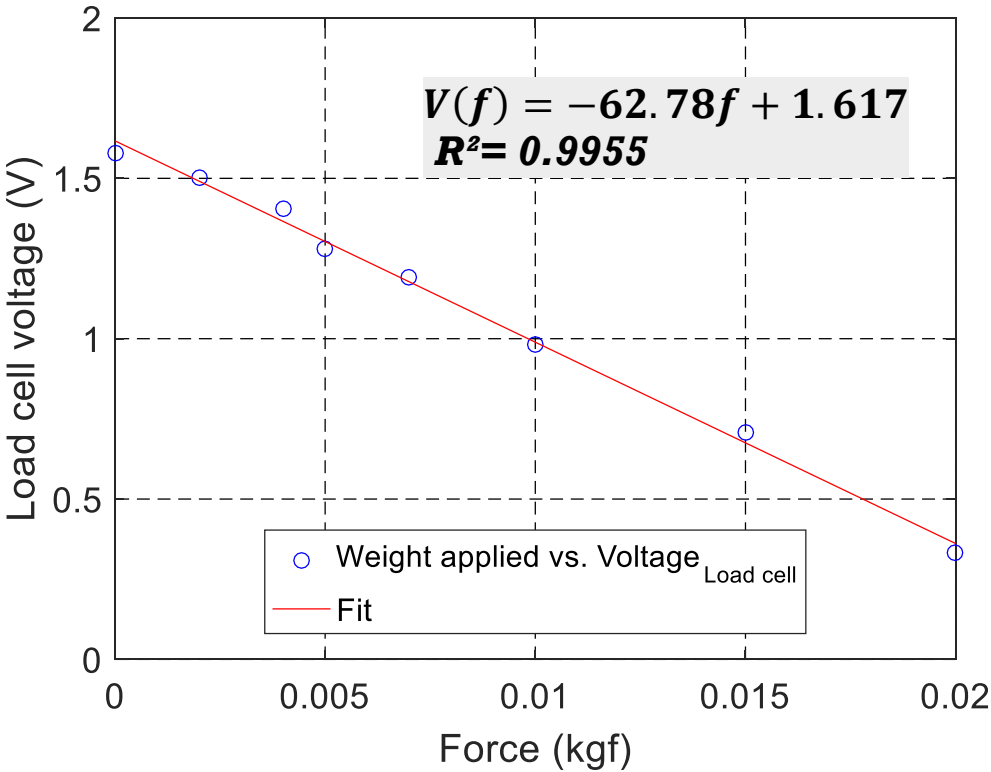
4.2.1 WEIGHT VS VOLTAGE

Figure 4.2: Weight vs voltage graph for load cell with error bars.

The force applied on the load cell in kilogram-force is plotted against the voltage obtained for the corresponding weight from the load- cell readout as shown in Figure 4.2. The data is obtained by calculating the mean of three different readings of voltage for weights ranging from $0 - 20g$. The curve shows a linearity with an R^2 of 0.9955.

4.2.2 VOLTAGE APPLIED TO DAQ VS LOAD CELL VOLTAGE

The variation in the voltage from the load cell- readout with the change in supplied voltage to the DAQ is as shown in Figure 4.3. The voltage readings are taken with the air pipe positioned at an angle of 30˚ to the load cell. The fit shows an exponential response of load cell voltage for every voltage applied to valve.
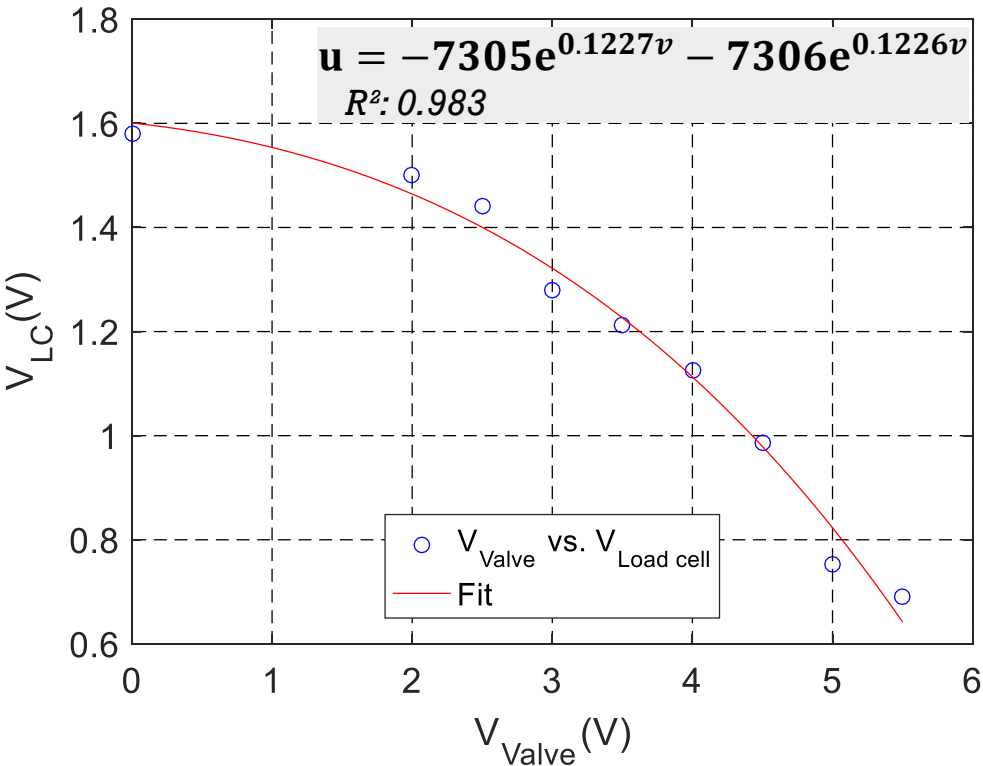

Figure 4.3: Voltage supplied to DAQ vs voltage from load cell

The fit equation shown in the figure:

$$u = -7305e^{0.1227v} - 7306e^{0.1226v}$$
$$R^2: 0.983$$

4.2.3 VOLTAGE SUPPLIED TO DAQ VS FORCE APPLIED

By correlating the data of weight vs voltage from load cell and Voltage to DAQ vs Voltage from load cell, the force applied by the air system is found out to be in the range of 0.6 - 14.7 gram-force. The force applied by the air system has an exponential response with voltage supplied to the air valve.
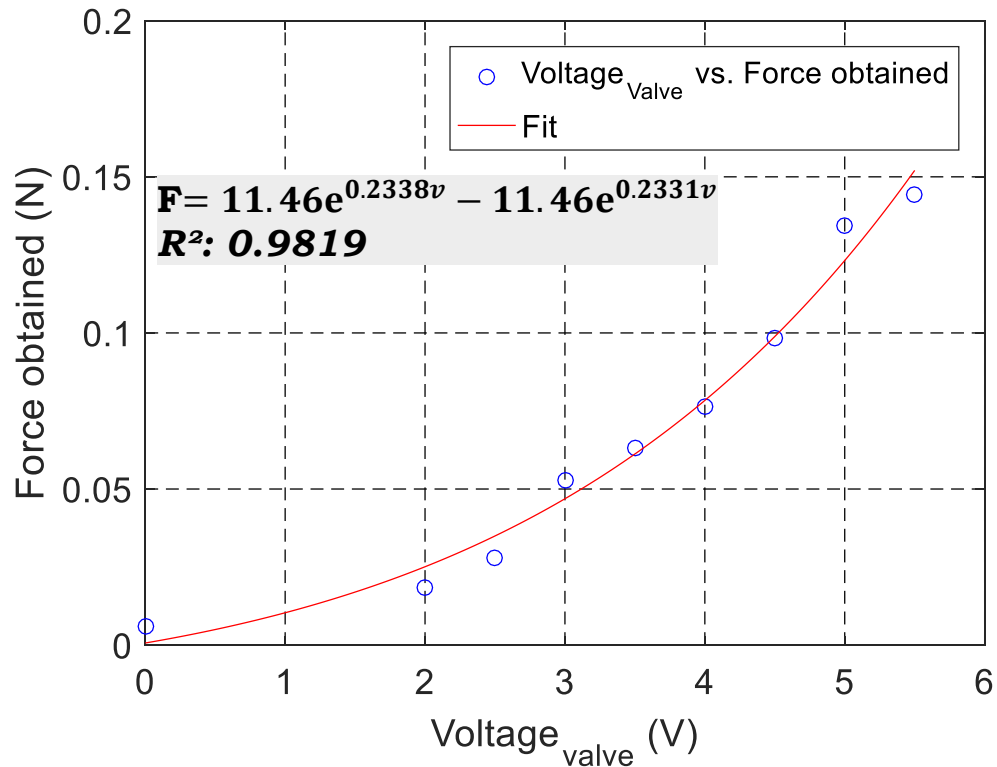
$$F= 11.46e^{0.2338v} - 11.46e^{0.2331v}$$
$$R^2: 0.9819$$

Figure 4.4: Voltage supplied to DAQ vs Force applied in Newton.

4.3 LABVIEW GUI

The LabVIEW GUI is designed and developed to interface the user with the CCD system and the control system. The fully developed GUI is as shown in Figure 4.5. The user is able to control the camera attributes directly from the GUI instead of controlling the attributes in NI MAX. The user is able to set the required frame rate for video recording and has the ability to choose between frame based acquisition or user defined timing.

Also the user has freedom over the amplitude and the frequency of the sinusoidal air pressure from the air system.
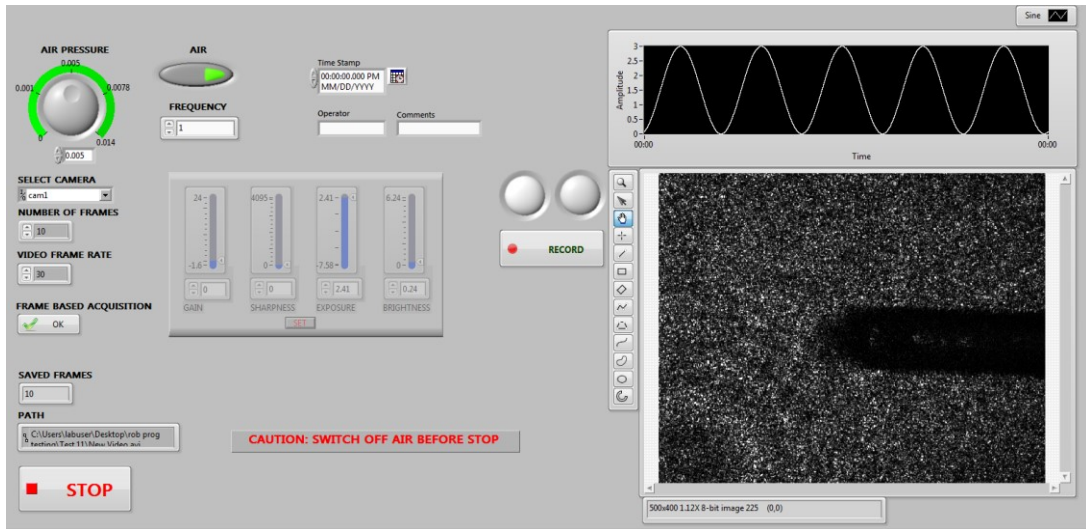
36

Figure 4.5: Optical elastography GUI

4.3.1 CONTROLLING THE AIR SYSTEM

The user can control the amplitude and frequency of the force exerted by the air system by the Air system control in GUI. The user is able to switch the Air system on or off with an LED button in the GUI. The air voltage knob and the frequency shifter is as shown in Figure 4.6. Also, the user can visualize the signal being sent to the air valve in the signal display monitor as shown in Figure 4.7.
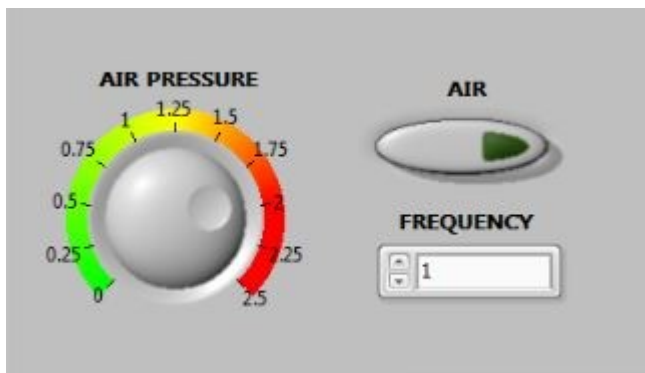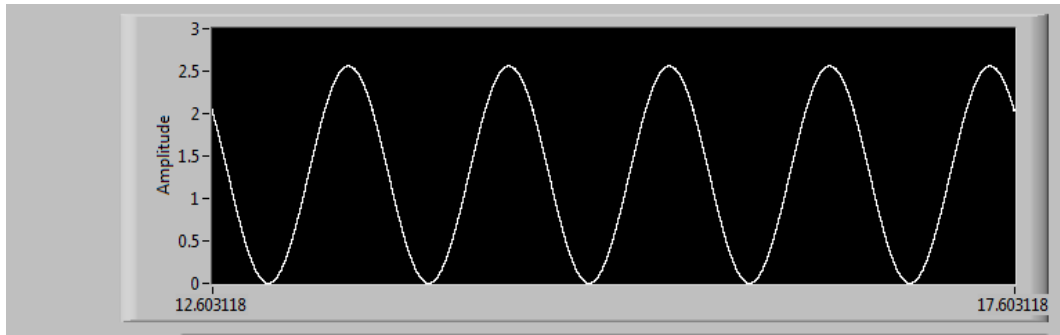

Figure 4.6: Air system control

Figure 4.7: Signal display monitor

4.3.2 CAMERA SELECTION

The GUI lets the user select the camera from the drop down menu as shown in Figure 4.8. The user is allowed to select either continuous image acquisition or acquire selected number of frames. The user can select the FRAME BASED ACQUISITION button for recording specified number of frames. The number of frames to be saved is set in the NUMBER OF FRAMES selection window and the playback frame rate for the video captured is set in the VIDEO FRAME RATE selection window.
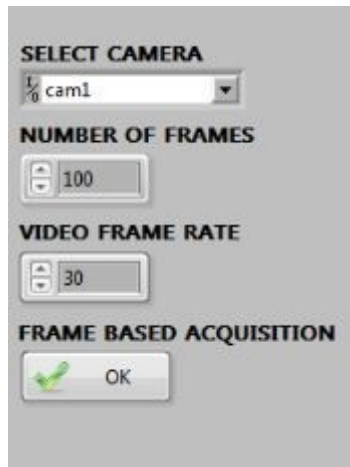

Figure 4.8: Frame based acquisition activation

4.3.3 CAMERA ATTRIBUTE SETTING

Camera attributes like gain, sharpness, exposure and brightness can be varied according to the requirement of the user and once done, the SET button is pressed to keep the attributes constant during the acquisition.
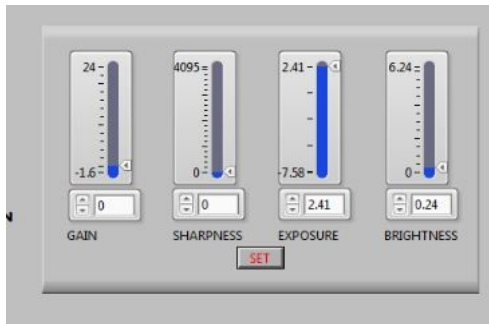

Figure 4.9: Camera attribute settings

4.3.4 FILE SELECTION AND USER COMMENTS

In the file selection window, the user can select the path for saving the images and video. It creates a default file named NEW VIDEO if no file name is specified, and rewrites the old file if the same name is found. The JPEG images get saved to the folder selected. Also, user can set comments and timestamp as in Figure 4.10.
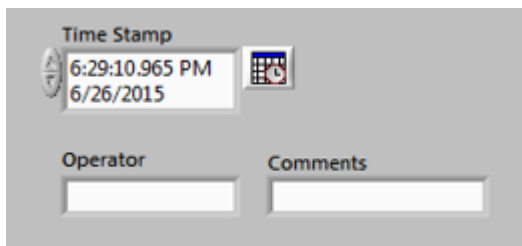

Figure 4.10: Time stamp and user comments.

4.3.5 RECORDING

When the RECORD button is pressed the image and video acquisition begins. If the Frame based acquisition mode is selected, the recording stops automatically after the specified number of frames are acquired. The green signal indicates that continuous acquisition mode is on and the user have to press the RECORDING button again to stop recording. Red signal shows that recording is on.
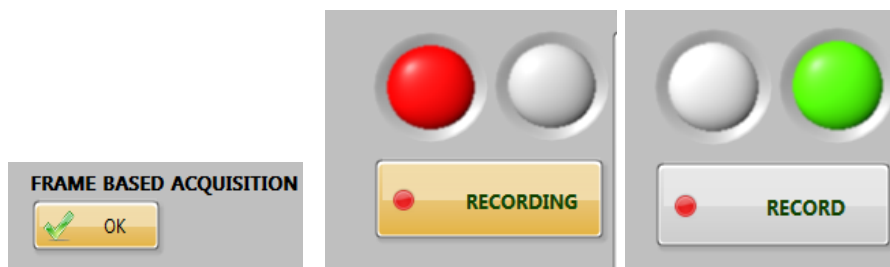

Figure 4.11: Different modes of Recording signals

4.2.6 IMAGE DISPLAY

Live feed of the region of interest is displayed in the display screen as shown in Figure 4.12. This enables the user to adjust the camera parameters and the position of the region of interest for imaging.
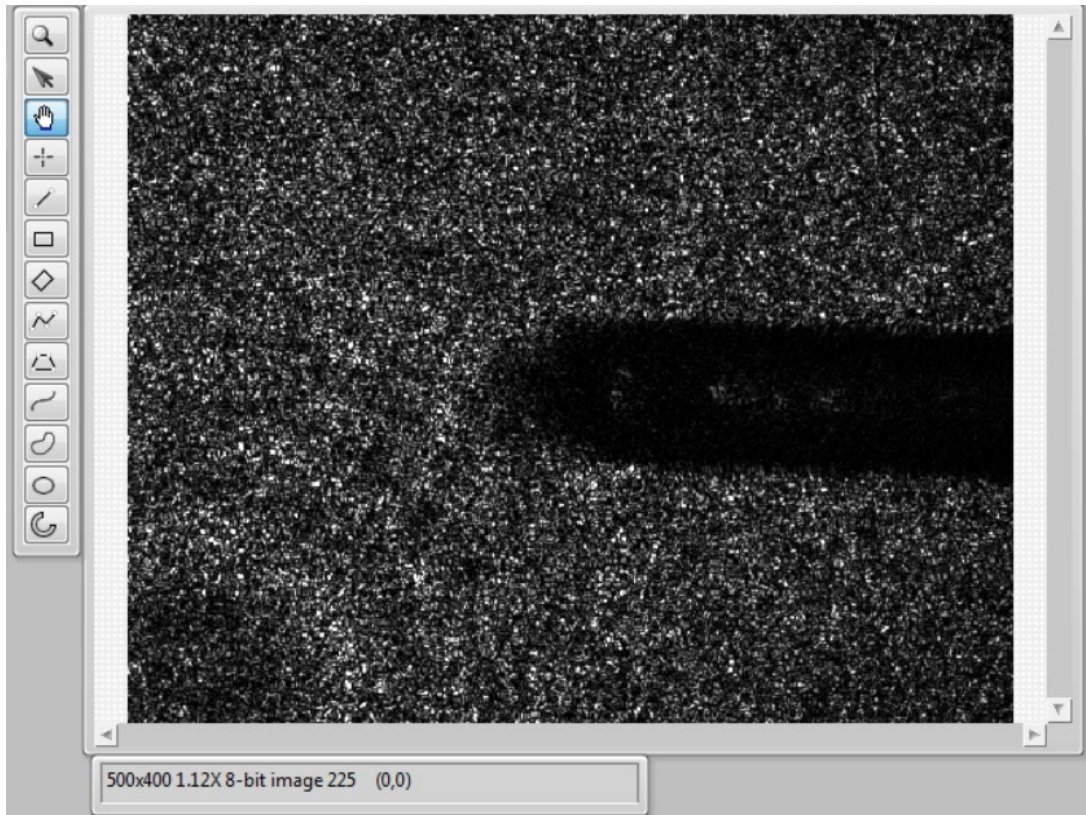
Figure 4.12: Live feed from the CCD is displayed in the window.

The total number of frames saved along with the location is displayed in the text diplay box in the GUI which is as shown in Figure 4.13.
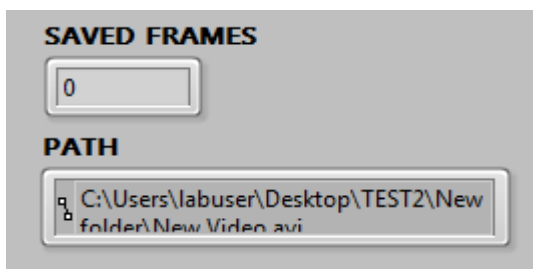

Figure 4.13: Information dialog box

4.4 OPTICAL ELASTOGRAPHY

The raw images were obtained without missing speckles in any frames. The resolution of the raw image is 320 X 240. This correspond

to 2 cm x 1.5 cm in the skin. Also, the time taken for capturing 200 frames was recorded as 0.5 seconds. This confirms that the images were acquired at a rate of 200 frames / second.
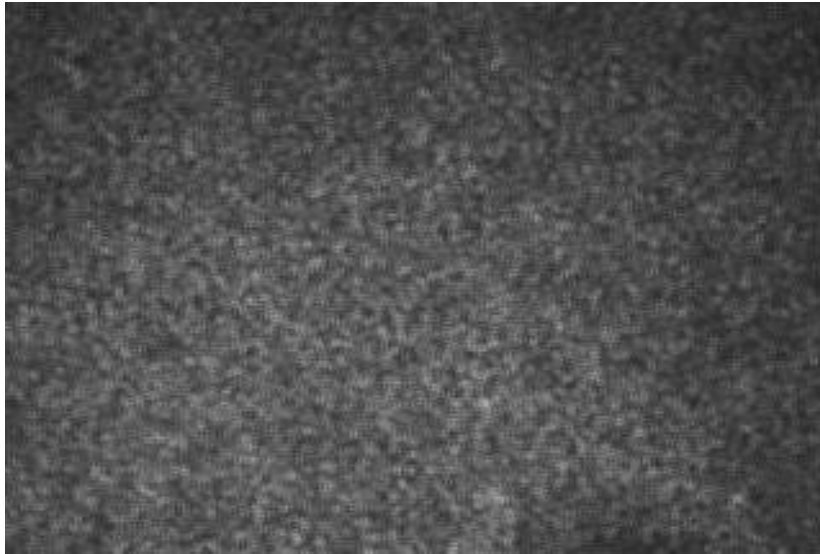

Figure 4.14: Raw image obtained for control skin with no application.

After processing the images obtained at 200 frames / second using the MATLAB code, the cumulative vector displacement is obtained as output.

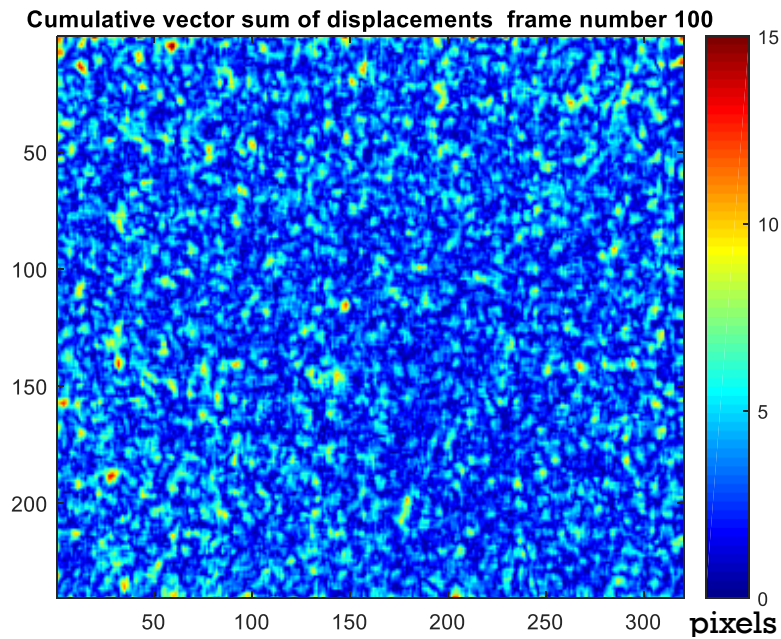**Cumulative vector sum of displacements frame number 100**

Figure 4.15: Cumulative vector sum displacement obtained after processing 200 images for control skin with no application.

The raw image after the application of serum on one half of the area being imaged is as shown in Figure 4.16. A total number of 200 images are taken during the deformation. The processed image after the application of the serum is as shown in Figure 4.17. The area on the right of the dotted lines is where the serum is applied. The color-bar denotes the displacement (in pixels) of speckles over 200 frames. The blue region denotes that the speckles have moved lesser distance in the range of 0-5 pixels / 200 frames and for the red region, the speckles have moved a greater distance in the range of $10 - 15$ pixels/ 200 frames.
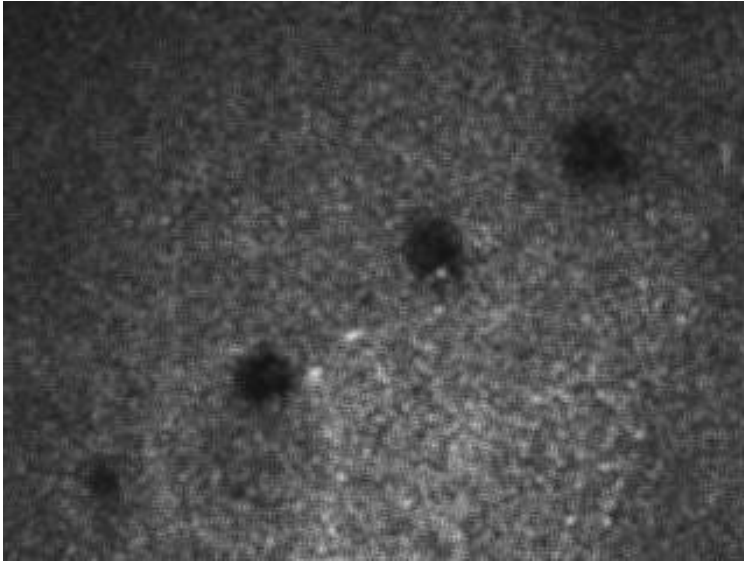
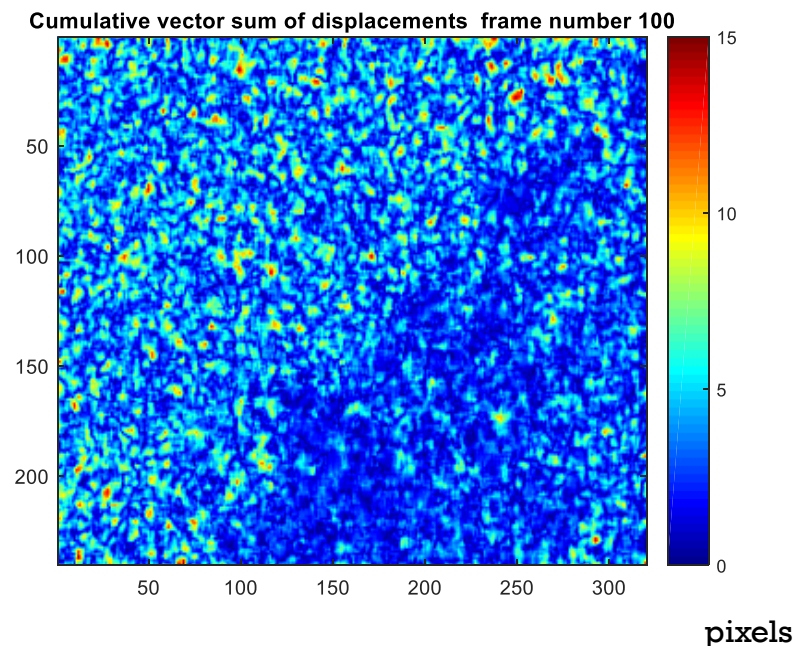*Figure 4.16: Raw image after application of serum*

Figure 4.17: Cumulative vector sum displacement mapping

CHAPTER 5

CONCLUSION AND FUTURE SCOPE

5.1 CONCLUSION

The objective of the work was to develop an optical elastography setup for studying the mechanical properties of skin. An optical elastography system with user controllable force application system and imaging system was developed. A user friendly LabVIEW GUI was designed and developed which enables the user to control the elastography system deftly.

5.1.1 AIR SYSTEM

The load cell used to study the force produced by the air system shows a high repeatability in Figure 4.1. The voltage produced by the load cell for different voltages supplied to the air valve has high accuracy. The deviations in the values might be due to load cell hysteresis. According to the readings the applied force from the air system ranges from 0- 0.15 N when the pipe is positioned at a distance of 1 cm from the region of interest or the focal plane of the camera. The user is able to vary the frequency and the amplitude of the sinusoidal air pressure instantaneously. This enables the user to vary the force applied on the region of interest during live recording.

5.1.2 IMAGING SYSTEM

The imaging system was setup perfectly where the user is able to control the camera attributes and the number of frames to be captured. The images were captured at 200 frames per second without loss of speckles during deformation. The images are of 320 x 240-pixel resolution and the imaged area is of size 1cm X 1.5 cm.

5.1.3 POST PROCESSING

The elastograms obtained after the application of a firming serum on the skin, as shown in Figure no. 4.15, shows that the difference in the displacement due to the air is distinguishable for the control and the applied region. The area with the serum applied shows lesser displacement when compared to the control region. The system is sensitive to differentiate between skin with different mechanical properties. The system is able to resolve between the region of greater displacement and lesser displacement.

5.2 FUTURE WORK

The MATLAB code which is used to process the images can be converted to an executable file which can be called by the LabVIEW GUI. With this, the user does not have to open MATLAB to process the images.

REFERENCES

1. Kirkpatrick, Sean J. "Optical Assessment of Tissue Mechanical Properties." *Saratov Fall Meeting'99*. International Society for Optics and Photonics, 2000.

2. Fung, Yuan-cheng. *Biomechanics: mechanical properties of living tissues*. Springer Science & Business Media, 2013.

3. Liang, Xing. *Coherence imaging technologies for the measurement of tissue and cell biomechanics*. Diss. University of Illinois at Urbana-Champaign, 2010.

4. Drakonaki, EE1, G. M. Allen, and D. J. Wilson. "Ultrasound elastography for musculoskeletal applications." *The British journal of radiology* (2014).

5. Bamber, Jeffrey, et al. "EFSUMB guidelines and recommendations on the clinical use of ultrasound elastography. Part 1: Basic principles and technology." *Ultraschall in der Medizin-European Journal of Ultrasound* 34.02 (2013): 169-184.

6. B.S. Garra, E.I. Cespedes, J. Ophir, S.R. Spratt, R.A. Zuurbier, C.M. Magnant, *et al.*
"Elastography of breast lesions: initial clinical results." Radiology, 202 (1) (1997), pp. 79–86

7. Silva, Glauber T., Alejandro C. Frery, and Mostafa Fatemi. "Image formation in vibro-acoustography with depth-of-field effects." *Computerized Medical Imaging and Graphics* 30.5 (2006): 321-327.

8. R.J. Dickinson, C.R. Hill "Measurement of soft tissue motion using correlation between A-Scans" Ultrasound Med Bio, 8 (3) (1982), pp. 263–271

9. Catheline, Stefan, et al. "Diffraction field of a low frequency vibrator in soft tissues using transient elastography." *IEEE transactions on ultrasonics, ferroelectrics, and frequency control* 46.4 (1999): 1013-1019.

10. Castéra, Laurent, et al. "Prospective comparison of transient elastography, Fibrotest, APRI, and liver biopsy for the assessment of fibrosis in chronic hepatitis C." *Gastroenterology* 128.2 (2005): 343-350.

11. Mariappan, Yogesh K., Kevin J. Glaser, and Richard L. Ehman. "Magnetic resonance elastography: a review." *Clinical anatomy* 23.5 (2010): 497-511.

12. Kennedy, Brendan F., Kelsey M. Kennedy, and David D. Sampson. "A review of optical coherence elastography: fundamentals, techniques and prospects." *IEEE Journal of Selected Topics in Quantum Electronics* 20.2 (2014): 272-288.

13. Kirkpatrick, Sean J., and Marilyn J. Cipolla. "High resolution imaged laser speckle strain gauge for vascular applications." *Journal of biomedical optics* 5.1 (2000): 62-71.

14. Kirkpatrick, Sean J., et al. "Imaging the mechanical stiffness of skin lesions by in vivo acousto-optical elastography." *Optics express* 14.21 (2006): 9770-9779.

15. Kennedy, Brendan F., et al. "Optical coherence micro-elastography: mechanical-contrast imaging of tissue microstructure." *Biomedical optics express* 5.7 (2014): 2113-2124.

16. Li, Xiang, et al. "Integrated IVUS-OCT imaging for atherosclerotic plaque characterization." *IEEE Journal of Selected Topics in Quantum Electronics* 20.2 (2014): 196-203.

17. Kuwahara, Y., et al. "Quantification of hardness, elasticity and viscosity of the skin of patients with systemic sclerosis using a novel sensing device (Vesmeter): a proposal for a new outcome measurement procedure."*Rheumatology* 47.7 (2008): 1018-1024.

18. Manschot, J. F. M., and A. J. M. Brakkee. "The measurement and modelling of the mechanical properties of human skin in vivo—II. The model." *Journal of Biomechanics* 19.7 (1986): 517-521.

19. Gallagher, A. J., Aisling Ní Annaidh, and Karine Bruyère. "Dynamic tensile properties of human skin." *IRCOBI Conference 2012, 12-14 September 2012, Dublin (Ireland)*. International Research Council on the Biomechanics of Injury, 2012.

20. Pailler-Mattei, C., S. Bec, and H. Zahouani. "In vivo measurements of the elastic mechanical properties of human skin by indentation tests." *Medical engineering & physics* 30.5 (2008): 599-606.

21. Boyer, Gaetan, et al. "Non-contact method for in vivo assessment of skin mechanical properties for assessing effect of ageing." *Medical engineering & physics* 34.2 (2012): 172-178.

22. Elsner, Peter, Enzo Berardesca, and Klaus-Peter Wilhelm, eds. *Bioengineering of the skin: skin biomechanics*. Vol. 5. Taylor & Francis US, 2001.

23. Escoffier, Catherine, et al. "Age-related mechanical properties of human skin: an in vivo study." *Journal of Investigative Dermatology* 93.3 (1989).

24. Rodnan, Gerald P., Esther Lipinski, and Joan Luksick. "Skin thickness and collagen content in progressive systemic sclerosis and localized scleroderma." *Arthritis & Rheumatism* 22.2 (1979): 130-140.

25. Hashimoto, Ken, and Tamotsu Kanzaki. "Cutis laxa: ultrastructural and biochemical studies." *Archives of dermatology* 111.7 (1975): 861-873.

26. Gogly, B., et al. "Morphometric analysis of collagen and elastic fibers in normal skin and gingiva in relation to age." *Clinical oral investigations* 1.3 (1997): 147-152.

27. Bernstein, Eric F., and Jouni Uitto. "The effect of photo-damage on dermal extracellular matrix." *Clinics in dermatology* 14.2 (1996): 143-151.

28. Dainty C (Ed), Laser Speckle and Related Phenomena, 1984, Sprinter Verlag, ISBN 0-387-13169-8

29. Boas, David A., and Andrew K. Dunn. "Laser speckle contrast imaging in biomedical optics." *Journal of biomedical optics* 15.1 (2010): 011109-011109.

30. Duncan, Donald D., and Sean J. Kirkpatrick. "Maximum-likelihood estimators for one-and two-dimensional speckle motion." *Biomedical Optics 2003*. International Society for Optics and Photonics, 2003.

31. Völz, H. "Frieden, BR, Probability, Statistical Optics, and Data Testing. A Problem Solving Approach. Berlin-Heidelberg-New York, Springer-Verlag 1983. XVII, 404 S., 99 Abb., DM 94, US $37.60. ISBN 3-540-11769-5 (Springer-Series in Information Sciences 10)." *ZAMM-Journal of Applied Mathematics and Mechanics/Zeitschrift für Angewandte Mathematik und Mechanik* 64.8 (1984): 340-340.

32. KAI-0340 IMAGE SENSOR, True sense imaging, Inc., Revision 1.0 PS-0024. July. 2012

33. Kirkpatrick, Sean J., Donald D. Duncan, and Elaine M. Wells-Gray. "Detrimental effects of speckle-pixel size matching in laser speckle contrast imaging." *Optics letters* 33.24 (2008): 2886-2888.

34. Nadkarni, Seemantini K., et al. "Characterization of atherosclerotic plaques by laser speckle imaging." *Circulation* 112.6 (2005): 885-892.

35. D 882 NPN Power transistor, ST Microelectronics, Inc., Revision 3. October. 2007